







Microestructura y propiedades dieléctricas de soluciones solidas tetragonales tipo $\text{Ba}_{1-3x}\text{Gd}_{2x}\text{Ti}_{1-3x}\text{Eu}_{4x}\text{O}_3$ ($x = 0.0, 0.0015, 0.01$ and 0.05 wt. %)

Microstructure and dielectric properties of tetragonal solid solutions type $\text{Ba}_{1-3x}\text{Gd}_{2x}\text{Ti}_{1-3x}\text{Eu}_{4x}\text{O}_3$ ($x = 0.0, 0.0015, 0.01$ and 0.05 wt. %)

R. Martínez-López ^{a*}, M. Pérez-Labra ^a, F. R. Barrientos -Hernández ^a, M. Reyes-Pérez ^a, M.U. Flores-Guerrero ^b and J. C. Juárez-Tapia ^a

^a Área Académica de Ciencias de la Tierra y Materiales, Universidad Autónoma del Estado de Hidalgo. Carretera Pachuca- Tulancingo Km 4.5 Mineral de la Reforma C.P. 42184, Hidalgo, México.

^b Área Electromecánica Industrial, Universidad Tecnológica de Tulancingo, C.P. 43642 Hidalgo, México.

Resumen

BaTiO_3 es un material ferroeléctrico con una estructura tipo perovskita ABO_3 . Este material es de gran interés debido a sus propiedades dieléctricas, magnéticas, ópticas, eléctricas, biomédicas, etc. Sus aplicaciones como electrocerámico incluyen, cerámicos piezoeléctricos, memorias cerámicas de acceso aleatorio, capacitores de disco, capacitores multicapa de fijación en superficie, sensores, filtros de telecomunicaciones, circuitos integrados, etc. Su alta constante dieléctrica permite diseñar dispositivos capacitores inteligentes y más pequeños. Las propiedades de BaTiO_3 se pueden mejorar en los procesos de síntesis, conformación y sinterización, al modificar composición química y microestructura con distintas técnicas como la activación mecánica, el dopaje, el prensado en frío, el control de la atmósfera, etc. En este trabajo se sintetizaron soluciones sólidas tipo $\text{Ba}_{1-3x}\text{Gd}_{2x}\text{Ti}_{1-3x}\text{Eu}_{4x}\text{O}_3$ con $x = 0, 0.0015, 0.01$ y 0.05 (% en peso) mediante el método de reacción en estado sólido. Los polvos precursores se secaron a 200°C , se descarboxaron a 900°C durante 12 horas y se sinterizaron a 1300°C durante 8 horas. Los patrones de difracción de rayos X (DRX) corresponden a BaTiO_3 tetragonal. La fase secundaria Eu_2TiO_5 en $x = 0.05$. Los espectros de los picos Raman mostraron los modos ferroeléctricos tetragonales característicos del BaTiO_3 , en las bandas de 716 cm^{-1} , 515 cm^{-1} , 305 cm^{-1} y 258 cm^{-1} en $x = 0, 0.0015$ y 0.01 . En 778 cm^{-1} se identificó una banda relacionada con la ocupación de iones Eu^{3+} en el BaTiO_3 . Se analizó la evolución estructural y las propiedades dieléctricas para determinar las mejores condiciones de sinterización ya que las propiedades eléctricas de los compuestos de BaTiO_3 dependen fuertemente de la microestructura y de la composición química. La muestra con $x = 0.0015$ registraron la permitividad relativa y capacitancia más alta de 100 Hz a 100 kHz a una temperatura de 105°C donde se determina la temperatura de Curie con una disminución de aproximadamente 20°C de acuerdo a lo reportado en la literatura. Lo que implica un rango de operación más amplio. La caracterización por MEB muestra granos con múltiples caras, alta cristalización y una estructura densa y heterogénea lo que está claramente relacionado con los valores de permitividad relativa alcanzados ya que el flujo de electrones y la retención de la carga no es afectada por el grado de porosidad, con la resistencia dieléctrica gracias a su alta densidad y la baja pérdida dieléctrica ya que el material resiste el deterioro gracias a su densidad.

Palabras Clave:

Dopaje, Dieléctrico, BaTiO_3 , Gadolinio, Europio

Abstract

BaTiO_3 is a ferroelectric material with an ABO_3 perovskite-type structure. This material is of great interest due to its dielectric, magnetic, optical, electrical, biomedical, etc. properties. Its applications as an electroceramic include piezoelectric ceramics, ceramic random-access memories, disk capacitors, surface-attached multilayer capacitors, sensors, telecommunications filters, integrated circuits, etc. Its high dielectric constant allows the design of smart and smaller capacitor devices. The properties of BaTiO_3 can be improved in the synthesis, forming, and sintering processes by modifying its chemical composition and microstructure with different techniques such as mechanical activation, doping, cold pressing, atmospheric control, etc. In this work, solid solutions of the $\text{Ba}_{1-3x}\text{Gd}_{2x}\text{Ti}_{1-3x}\text{Eu}_{4x}\text{O}_3$ type with $x = 0, 0.0015, 0.01$ and 0.05 (wt%) were synthesized by the solid-state reaction method. The precursor powders were dried at 200°C , decarbonated at 900°C for 12 hours and sintered at 1300°C .

*Autor para la correspondencia: ricardo.martinez@uaeh.edu.mx

Correo electrónico: miguel_perez5851@uaeh.edu.mx (Miguel Pérez-Labra), frbh68@hotmail.com (Francisco Raúl Barrientos-Hernández), mreyes@uaeh.edu.mx (Martín Reyes Pérez), mflores@utectulancingo.edu.mx (Mizraim Uriel Flores-Guerrero), jcuarez@uaeh.edu.mx (Julio Cesar Juárez-Tapia).

for 8 hours. The X-ray diffraction (XRD) patterns correspond to tetragonal BaTiO₃. The secondary phase Eu₂TiO₅ at $x = 0.05$. The Raman peak spectra showed the characteristic tetragonal ferroelectric modes of BaTiO₃, in the bands of 716 cm⁻¹, 515 cm⁻¹, 305 cm⁻¹ and 258 cm⁻¹ at $x = 0, 0.0015$ and 0.01 . At 778 cm⁻¹ a band related to the occupation of Eu³⁺ ions in BaTiO₃ was identified. The structural evolution and dielectric properties were analyzed to determine the best sintering conditions since the electrical properties of BaTiO₃ compounds strongly depend on the microstructure and chemical composition. The sample with $x = 0.0015$ recorded the highest relative permittivity and capacitance from 100 Hz to 100 kHz at a temperature of 105 °C where the Curie temperature is determined with a decrease of approximately 20 °C according to what has been reported in the literature. This implies a broader operating range. SEM characterization reveals multifaceted grains, high crystallization, and a dense, heterogeneous structure. This is clearly related to the relative permittivity values achieved, since electron flow and charge retention are not affected by the degree of porosity. It also has a high dielectric strength thanks to its high density, and a low dielectric loss, since the material resists deterioration thanks to its density.

Keywords:

Doping, Dielectric, BaTiO₃, Gadolinium, Europium

1. Introduction

1.1. Barium titanate (BaTiO₃) is an ABO₃ type ferroelectric perovskite that exhibits a Curie temperature (~120°C), high dielectric constant, large mechanical-quality factor, large pyroelectric coefficient, nontoxic handling and low cost of manufacturing, (Lingxian S. et al., 2025), features for which the BaTiO₃ based ceramic compounds have been strong candidate for several electronic applications (Uchino, 2018). It is well known that the ferroelectricity in BaTiO₃ is due to a displacement of the Ti atoms and the effect is very sensitive to interatomic distances (lattice parameter) (Kacimi-Naciri H. et al., 2025). The electrical properties of BaTiO₃ compounds largely depend on their microstructure, chemical compositions (Xu D. et al., 2025) as well as the appropriate amount of doping in the BaTiO₃ host. To expand the applications of electroceramic materials or improve existing ones, special attention must be paid to the sintering and forming processes of the devices. A widely used technique to improve the dielectric properties of materials is doping. In doping, ion occupancy at A or B sites in ABO₃ structures modifies the Curie temperature and other physical properties (Yu-Lin D. et al., 2025). The addition of electron-donating doping elements is intended to create semiconductor regions within the BaTiO₃ grains. If the replacement cation has a lower valence than the original, electron holes could be released, and if the replacement cation has a higher valence, electrons could be released (Jang S. et al., 2020). Particularly, the elements gadolinium and europium, (trivalent lanthanide elements) have been investigated separately as dopants in BaTiO₃. Ruf T., et al., (2022) prepared Gd-doped BaTiO₃ thin films by pulsed laser deposition to increase the fine crystallinity, enhancing the characteristics of the devices by controlling their properties. Furthermore, it has been reported that Gd³⁺ doping could change thermal conductivity for its reduction, making it a promising material for photo thermoelectric conversion (Du Y., Li J., Wang J., 2025). On the other hand, the inclusion of europium into the host lattice of BaTiO₃ is scarcely found in the literature. Europium is the most reactive rare earth element, exhibits unusual metallurgical properties, and has been reported to be an efficient photoluminescence sensitizer in perovskites and related materials (Lefevre et al., 2018). The valence state and the radius ionic of Gd³⁺ ion and Eu³⁺ (1.215 Å with coordination number 12 and 1.226 Å with coordination number 12 respectively) are intermediate between those of Ba²⁺ ion (1.42 Å) and Ti⁴⁺ ion (0.61 Å). As a result, theoretically Gd³⁺ and Eu³⁺ ions can occupy either A or B site, depending on Ba/Ti mole ratio (Yu-Lin D. et al., 2025). To determine the optimal sintering conditions for solid

solutions based on BaTiO₃ dielectric properties, taking into account measured values of relative permittivity and capacitance, the microstructure and chemical composition of the solutions were analyzed, taking into account density, grain morphology, and concentration of the doping element gadolinium. This was done with the aim of improving the properties of undoped BaTiO₃.

2. Experimental

Samples of BaTiO₃ doped with Gd³⁺ and Eu³⁺ were prepared according to; Ba_{1-3x}Gd_{2x}Ti_{1-3x}Eu_{4x}O₃, ($x = 0.0, 0.0015, 0.01, 0.05$ Gd³⁺, Eu³⁺ (wt. %)) using the solid state reaction method; grinding, BaCO₃ (Sigma-Aldrich cas No. 513-77-9, 99.9%), TiO₂ (Sigma-Aldrich, cas No.13463-67-7 99.9%), Gd₂O₃ (Sigma-Aldrich, cas No. 278513-25G 99.9%) and Eu₂O₃ (Sigma-Aldrich, cas No. 1308-96-9, 99.9%) in a agate mortar employing acetone as a control medium. The precursors powders firstly were dried at 200°C, before weigh each powder sample was placed in a platinum crucible and was decarbonated at 900°C for 12 hours employing 4°C/min as a heating rate and subsequently was regrinding for 40 min in agate mortar. After that they were placed in a platinum crucible and were sintered at 1300 °C for 8 hours using 4°C/min as a heating rate in a muffle furnace (Thermolyne model 46200). The structural evolution of the products was monitored by X-ray diffraction (diffractometer Equinox 2000 Cu K α). After the phase was obtained the powder mixtures were compacted using a uniaxial pressing at 250 MPa in an 8-mm stainless steel die to produce 3 mm thick green pellets which were sintered at 1300 °C for 8 hours in air atmosphere with heating and cooling rates of 4 °C / min. Later, they were sanded, polished and cleaned in an ultrasonic bath. Platinum paste was painted on opposite surfaces of the pellets to form electrodes. A thin platinum strip was then applied to the platinum electrodes to act as a contact. Pellets were mounted in a conductivity jig which was inserted in a tube furnace. The capacitance data were used to get permittivity data. Electrical measurements were performed on LC Meter Analyzer ELC -3133A LCM Escort, at 100 Hz, 120Hz, 1KHz, 10KHz y 100 KHz. The morphology studies were performed in a JEOL JSM-670 IF Field Emission Scanning Electron Microscope (Jeol, Tokyo, Japan). Additionally, Raman studies were carried out for each powder samples using a Perkin Elmer Spectrum Gx spectrophotometer, (Überlingen, Germany), with neodymium laser (1064 nm) excitation.

3. Results and discussion

3.1. X-Ray diffraction

XRD patterns of sintered samples with different dopant contents are shown in Figure 1. A combination of tetragonal BaTiO_3 (JCPDS 961507757) and orthorhombic Eu_2TiO_5 phases (JCPDS 962002716), with the first one being predominant. The presence of the tetragonal phase, which exhibits ferroelectric properties, can be observed at the positions $2\theta \approx$ to 26.05, 36.99, 45.78, 53.14, 60.31, 66.38, 78.67, 84.34, 89.72 and 90.64. From the undoped composition ($x=0$) to the doped composition with $x = 0.01$, the tetragonal phase BaTiO_3 (JCPDS 961507757) is presented, which indicates the doping elements gadolinium and europium have been integrated into the BaTiO_3 structure, increasing the concentration of doping elements creates changes in the crystal structure depending on the substitution mechanism and can expand or contract the BaTiO_3 structure, furthermore, when the concentration of Gd^{3+} and Eu^{3+} was $x = 0.05$, the Europium titanate (Eu_2TiO_5) secondary phase was identified (JCPDS 962002716). Eu_2TiO_5 has been successfully used in the PM-1 reactor as a control rod material (Syamala et al., 2008). The formation of the Eu_2TiO_5 phase indicates that the solubility limit of Eu^{3+} in the BaTiO_3 structure was reached when x was equal to 0.05. On the other side, as far as europium is concerned, no secondary phases with europium in its structure were identified. The concentration of the doping elements is crucial as they determine the phase present and/or the combination of phases, and therefore the properties that the electroceramic material will have.

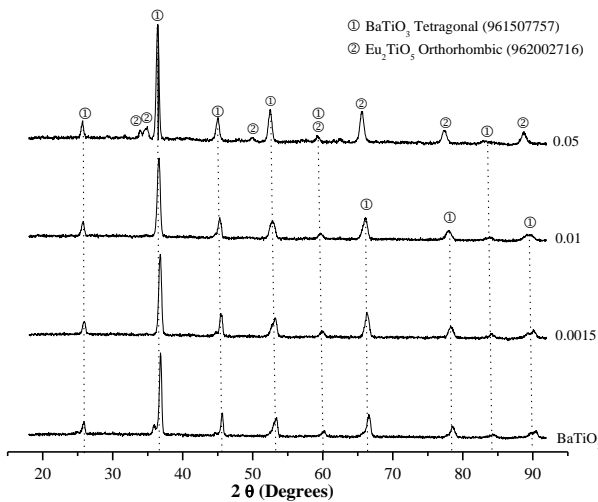


Figure 1: XRD diffractograms for $\text{Ba}_{1-3x}\text{Gd}_{2x}\text{Ti}_{1-3x}\text{Eu}_{4x}\text{O}_3$ powders sintered at 1300°C for 8 h for different values of x .

3.2. Raman spectroscopy (RS)

Figure 2 shows the evolution of the Raman spectra at room temperature of powders sintered at 1300°C , with different concentrations of Gd^{3+} and Eu^{3+} for $0.0015 \leq x \leq 0.05$. In the image can be observed a weak peak around 716 cm^{-1} for the spectra with $x = 0$ (BaTiO_3), 0.0015 and 0.01, a sharp peak at 305 cm^{-1} , and two broad peaks around 258 and 515 cm^{-1} . This Raman spectra of powders for polycrystalline BaTiO_3 are consistent with the tetragonal BaTiO_3 found in literature. The peak around 715 cm^{-1} is associated with the mode LO of A_1 symmetry, this has been reported as the highest frequency longitudinal optical. The peaks around 260 cm^{-1} and 515 cm^{-1} are assigned to the TO modes of A_1 symmetry, likewise, the band around 305 cm^{-1} has been assigned to the B1 mode (Huangfu G., et al., 2023). The presence of a new

band close to 778 cm^{-1} mode was also identified for the Raman spectrum of the sample with $x = 0.05\text{ Gd}^{3+}$ and Eu^{3+} (wt. %). It has been reported (Lu et al., 2013), that this band relates to the occupation of Eu^{3+} ions at BaTiO_3 ceramics with a single-phase structure, so it can be inferred that the 778 cm^{-1} band is attributed to the presence of the Eu_2TiO_5 phase identified by XRD technique (Figure 1).

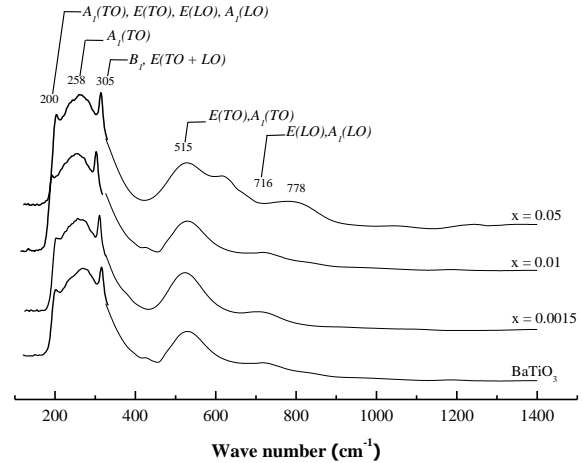


Figure 2: Raman spectra of powders sintered at 1300°C , $0 \leq x \leq 0.05$.

3.3. Dielectric and ferroelectric measurements

$\text{Ba}_{1-3x}\text{Gd}_{2x}\text{Ti}_{1-3x}\text{Eu}_{4x}\text{O}_3$ capacitors were prepared by applying platinum paste to opposite surfaces of the sintered pellets to form electrodes and placing a platinum strip over the platinum electrodes to act as a contact. Figure 3 a) shows the maximum values of relative permittivity (k) and the maximum values of capacitance (b)), that the samples reached a range of 20 to 200°C , and the temperature at which these maximums were reached is specified on the upper x -axis, for each sample manufactured in the range of $0 \leq x \leq 0.05$ (on the lower x -axis) evaluated at 100 Hz, 120Hz, 1KHz, 10KHz y 100 KHz. The sample with $x = 0.0015$ registered the highest relative permittivity values in each of the frequencies evaluated (Figure 3 a)), however, the relative permittivity values decreased for the sample with $x = 0.01$. Borah et al (Borah et al., 2014), reported that the dielectric constant showed a tendency to decrease with the increasing of dopant content and frequency (results obtained at 1KHz were reported) in Gd^{3+} doping BaTiO_3 pseudo-cubic nanostructures when the Gd-doping level varied between 0 and 7 %. In our research, for the sample with $x = 0.05$ low relative permittivity values were recorded. The graphs permittivity versus temperature of the sample with $x = 0.05$ (Figure 3 c) were characterized by low intensity and amplitude of the peaks suggesting a mixture of phases coexisting in the material. This possibility is supported by the results from XRD (Figure 1) and Raman spectra (Figure 2) for the same sample. The paraelectric behavior is evident (Hernández et al., 2014) and it is highlighted that the dopant concentration must be controlled to obtain the desired properties in the material. The Curie main peak changes from 110°C to 100°C suggest that cubic phase is becoming more stable (Hernández et al., 2014). This is an advantage by increasing the maximum operating range of the device.

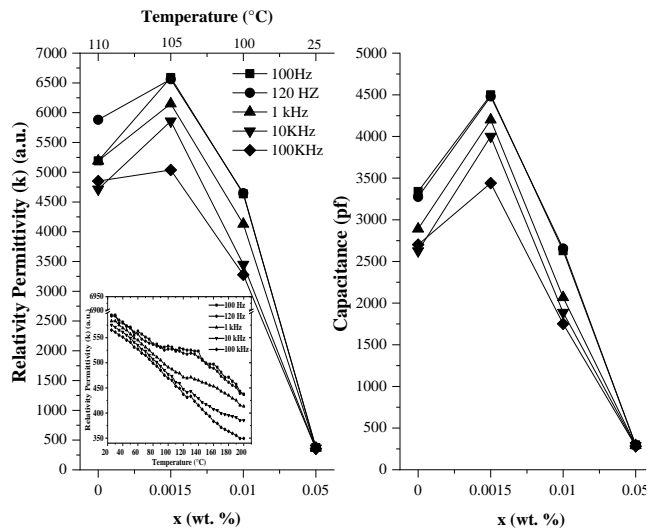


Figure 3: a) Relative permittivity against x (wt.%), b) capacitance against x (wt.%) and c) Relative permittivity against temperature $x = 0.05$ (wt.%) of capacitors prepared from $\text{Ba}_{1-3x}\text{Gd}_{2x}\text{Ti}_{1-3x}\text{Eu}_{4x}\text{O}_3$ to 100Hz, 120Hz, 1KHz, 10KHz y 100KHz.

3.4. Morphology and microstructure

Figure 4 a-d shows SEM images of Gd^{3+} and Eu^{3+} doped BaTiO_3 for the samples sintered at 1300°C with different gadolinium and europium concentrations. The samples consisting mainly of the grains whose shape, characterized by many faces, suggests a high crystallization level and also show a dense and inhomogeneous structure with mean grain size of $0.93 \mu\text{m}$ for $x = 0$ (Figure 4 a)), $0.61 \mu\text{m}$ for $x = 0.0015$ (Figure 4 b)), $0.41 \mu\text{m}$, for $x = 0.01$ (Figure 4 c)) and $0.58 \mu\text{m}$ for $x = 0.05$ (Figure 4 d)). It was observed that the inclusion of gadolinium and europium in the structure of BaTiO_3 produces a decrease in the average grain size (Figure 4 b-c)) subsequently increases (Figure 4 d)). It has been reported (Kingery et al., 1976) that when the process is controlled and the grain size is $1.5 \mu\text{m}$ or less, no 90° domains are formed. Therefore, the material maintains residual stresses and the dielectric constant has a high value. Some pores located at grain boundaries were observed for the samples with $x = 0.0015$, 0.01 and 0.05 (Figure 4 b-d)). With the decrease in the average grain size from $0.93 \mu\text{m}$ in the undoped composition ($x = 0$) to $0.61 \mu\text{m}$ in the first doped composition ($x = 0.0015$), the highest values of relative permittivity and capacitance were presented. Subsequently, from the composition $x = 0.0015$ to the composition $x = 0.01$, a decrease in the average grain size to $0.41 \mu\text{m}$ was presented, but the relative permittivity and capacitance values dropped to levels even lower than those of the undoped composition ($x = 0$). Finally, in the composition $x = 0.05$, where the secondary phase Eu_2TiO_5 is present, the material behaves in a paraelectric manner. Images obtained by SEM show that the microstructure is not drastically affected by gadolinium and europium doping.

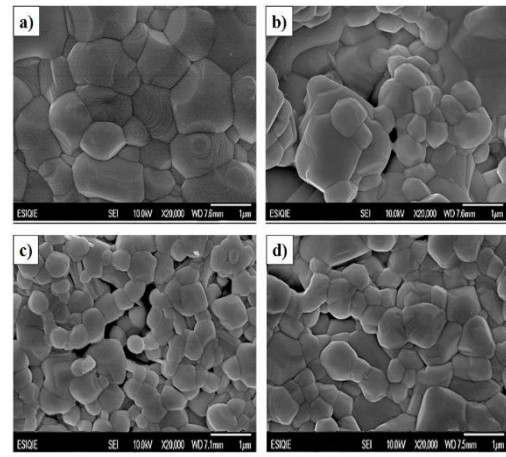


Figure 4: SEM micrographs of BaTiO_3 , with different gadolinium and europium concentrations: a) $x = 0$, and b) $x = 0.0015$, c) 0.01 and d) 0.05 .

4. Conclusions

Solid solutions type $\text{Ba}_{1-3x}\text{Gd}_{2x}\text{Ti}_{1-3x}\text{Eu}_{4x}\text{O}_3$ with $x = 0.0$, 0.0015 , 0.01 and 0.05 (wt. %) were investigated by XRD, RS, electric measurements and SEM techniques. XRD results confirmed the presence of BaTiO_3 tetragonal phase mainly at the positions $2\theta \approx 20.26, 26.05, 36.99, 45.78, 53.14, 66.38$, and 78.67 , this phase exhibits ferroelectric properties. The secondary phase Eu_2TiO_5 when the concentration of Gd^{3+} and Eu^{3+} was $x = 0.05$ was identified. No secondary phases with europium in its structure were identified. The Raman results showed the characteristic Raman peaks of the tetragonal BaTiO_3 ferroelectric phase located in the modes 716 cm^{-1} , 515 cm^{-1} , 305 cm^{-1} , and 258 cm^{-1} for spectra with $x = 0$ (BaTiO_3), 0.0015 and 0.01 . A band around 778 cm^{-1} , related to the occupation of Eu^{3+} ions in BaTiO_3 was identified for the sample with $x = 0.05$. The SEM results showed grains whose shape, was characterized by many faces, with high crystallization level and a dense and inhomogeneous structure with mean grain size of $0.93 \mu\text{m}$ for $x = 0$, $0.61 \mu\text{m}$ for $x = 0.0015$, $0.41 \mu\text{m}$, for $x = 0.01$ and $0.58 \mu\text{m}$ for $x = 0.05$. The sample with $x = 0.0015$ registered the highest relative permittivity and capacitance values in each of the frequencies evaluated, this is attributed to the average grain size, the formation of multiple ferroelectric domains, to its high densification and low porosity observed in SEM, and to the incorporation of the doping elements gadolinium and europium into the BaTiO_3 structure confirmed by XRD and Raman. Furthermore, the Curie temperature reached at 105°C is notable, allowing for a broader operating range, compared to the undoped phase and the phases with higher dopant content.

Acknowledgment

The authors thank SECIHTI-Mexico and the Hidalgo Science, Technology and Innovation Council (CITNOVA) for financial support and the Autonomous University of the State of Hidalgo, Mexico, for technical support.

Conflict of interests

The authors declare that there are no conflicts of interest.

Referencias

- Borah, M., & Mohanta, D. (2014). Effect of Gd^{3+} doping on structural, optical and frequency-dependent dielectric response properties of pseudo-cubic $BaTiO_3$ nanostructures. *Applied Physics A*, 115(3), 1057-1067. DOI:10.1007/s00339-013-7941-7
- Du Y., Li J., Wang J., (2025). Relationship between thermoelectric properties and infrared emissivity of Gd-doped $SrO(SrTiO_3)_2$. *Journal of the European Ceramic Society*, 45(5), 117112. DOI: 10.1016/j.jeurceramsoc.2024.117112
- Hernández, F. B., Hernández, I. L., Yáñez, C. G., Flores, A. A., Sierra, R. C., & Labra, M. P. (2014). Structural evolution of $Ba_8Ti_3Nb_4O_{24}$ from $BaTiO_3$ using a series of $Ba(Ti_{1-5x}Nb_{4x})O_3$ solid solutions. *Journal of Alloys and Compounds*, 583, 587-592. DOI: 10.1016/j.jallcom.2013.09.016
- Huangfu G., et al. (2023). Investigation of lattice evolutions of tetragonal ($Na_{0.5}Bi_{0.5}$) TiO_3 - $BaTiO_3$ single crystal by phonon modes in Raman scattering, *Scripta Materialia*, 225, 115184. DOI: 10.1016/j.scriptamat.2022.115184.
- Jang S., et al. (2020). A-site and B-site substitutions and the emission properties of Eu^{3+} ions in ABO_3 -type cubic perovskite: A case study of $BaZrO_3$. *Current Applied Physics*, 20(10), 1110-1117. DOI: 10.1016/j.cap.2020.07.011.
- Kacimi-Naciri H., et al. (2025). DFT-based and experimental study on Sr-doped $BaTiO_3$: Impacts on piezoelectric and ferroelectric performance. *Ceramics International*, 51(17), 23801-23813. DOI: 10.1016/j.ceramint.2025.03.069.
- Lefevre, G., Herfurth, A., Kohlmann, H., Sayede, A., Wylezich, T., Welinski, S., & Kunkel, N. (2018). Electron-Phonon Coupling in Luminescent Europium-Doped Hydride Perovskites Studied by Luminescence Spectroscopy, Inelastic Neutron Scattering, and First-Principles Calculations. *The Journal of Physical Chemistry C*, 122(19), 10501-10509. DOI: 10.1021/acs.jpcc.8b01011
- Lingxian S., et al. (2025). Enhanced piezoelectric response and Curie temperature of $BiFeO_3$ - $BaTiO_3$ by substituting $PbTiO_3$ for $BaTiO_3$. *Ceramics International*, 51(18 – A), 24945-24951. DOI: 10.1016/j.ceramint.2025.03.175
- Lu, D. Y., Zhang, L., & Sun, X. Y. (2013). Defect chemistry of a high-k ‘ Y_5V ’ ($Ba_{0.95}Eu_{0.05}$) TiO_3 ceramic. *Ceramics International*, 39(6), 6369-6377. DOI: 10.1016/j.ceramint.2013.01.063
- Uchino, K. (2018). *Ferroelectric devices*. Marcel Dekker, New York, 2000. CRC press. DOI: 10.1201/b15852, ISBN: 13: 978-1-4398-0376-9
- Ruf T., et al. (2022). Preferential growth of perovskite $BaTiO_3$ thin films on $Gd_3Ga_5O_{12}(100)$ and $Y_3Fe_5O_{12}(100)$ oriented substrates by pulsed laser deposition. *Materials Advances*, 3(12), 4920-4931. DOI: 10.1039/d2ma00041e
- Syamala, K. V., Panneerselvam, G., Subramanian, G. G. S., & Antony, M. P. (2008). Synthesis, characterization and thermal expansion studies on europium titanate (Eu_2TiO_5). *Thermochemical Acta*, 475(1-2), 76-79. DOI: 10.1016/j.tca.2008.05.008
- Xu D., et al. (2025). The influences of defect-induced phase transition on the morphology structure and electrical properties of Ni/Zn doped $BaTiO_3$ ceramics. *Ceramics International*. DOI: 10.1016/j.ceramint.2025.06.430
- Yu-Lin D. et al. (2025). Understanding the effect of rare-earth doping in ABO_3 ferroelectrics on capacitive energy storage. *Journal of the European Ceramic Society*, 45(14), 117539. DOI: 10.1016/j.jeurceramsoc.2025.117539